Probing the Limit of Weak Host–Guest Interactions: Insertion Compounds of Mercury(II) Halides with Microporous SiO_2 Hosts

Gernot Wirnsberger,[a] Bernhard M. Pillep,[b] Alois Popitsch,[a] Peter Knoll,[c] and Peter Behrens*[b]

Dedicated to Professor Wolfgang Metz on the occasion of his 65th birthday

Abstract: Mercury(II) halides HgX_2 (X = Cl, Br, I) were inserted into the voids of the crystalline microporous SiO_2 modifications deca-dodecasil 3R (short term: DDR), *silica*-theta-1 (TON), *silica*-ferrierite (FER) and silicalite-1 (MFI) by vapour phase loading. The properties of the occluded guest species were studied by X-ray absorption spectroscopy (X-ray absorption near-edge structure (XANES) and extended X-ray absorption fine structure (EXAFS) analysis), UV/Vis spectroscopy, and IR and Raman spectroscopy. The methods reveal the presence of HgX_2 molecules in the insertion compounds. The interactions between these electroneutral guest molecules and the electroneutral surrounding SiO_2 framework are weak. In addition, no indication of any significant guest–guest interaction between the embedded molecules was found, in contrast to the analogous iodine insertion compounds, where these become more important with increasing pore dimensionality (G. Wirnsberger et al., Angew. Chem. **1996**, *108*, 2951–2953; *Angew. Chem. Int. Ed. Engl.* **1996**, *35*, 2777). Analysis of the HgL_3 EXAFS confirms a coordination number of two for Hg and gives Hg–X bond lengths of 2.26 ± 0.02, 2.38 ± 0.02 and 2.57 ± 0.02 Å for the trapped $HgCl_2$, $HgBr_2$ and HgI_2 molecules, respectively. These values are very close to those of the corresponding molecules in the vapour phase and are the shortest determined for HgX_2 molecules in solid-state compounds to date (a comparably short distance only appears in the recently reported $[Cu(2\text{-pyrazinecarboxylato})_2\text{-}HgI_2] \cdot HgI_2$ with $d(Hg–I) = 2.577(2)$ Å; Dong et al., *Angew. Chem.* **2000**, *112*, 4441–4443; *Angew. Chem. Int. Ed.* **2000**, *39*, 4271). Thus, there emerges a picture of almost unperturbed HgX_2 molecules, similar to those in the vapour phase or in non-coordinating solvents, in a solid crystalline matrix of high temperature stability, a very unusual state of matter. Despite the weakness of the host–guest interactions, investigations on small crystallites of the HgX_2–TON composites using a Raman microscope show a strong polarization dependence, providing evidence for an orientational alignment of the HgX_2 molecules inside the one-dimensional pore system of this host. For these reasons, the host matrices used in this study can be viewed as orienting solid solvents, coordinating only very weakly to the inserted HgX_2 guest molecules, but exhibiting a strong geometrical template function for their alignment. The concept of using electroneutral SiO_2 modifications as host components for a modular construction of new host–guest compounds thus allows the designed construction of ordered guest assemblies, with the pore systems of the rigid host matrices acting as space-confining and ordering templates for the guest components.

Keywords: host–guest systems · insertion compounds · mercury · porosils · zeolite analogues

[a] Dr. G. Wirnsberger, Prof. Dr. A. Popitsch
Institut für Anorganische Chemie der Universität Graz
Schubertstrasse 1, 8010 Graz (Austria)

[b] Prof. Dr. P. Behrens, Dr. B. M. Pillep
Institut für Anorganische Chemie, Universität Hannover
Callinstrasse 9, 30167 Hannover (Germany)
Fax: (+49) (0)511-762-3660
E-mail: peter.behrens@mbox.acb.uni-hannover.de

[c] Prof. Dr. P. Knoll
Institut für Experimentalphysik der Universität Graz,
Universitätsplatz 5, 8010 Graz (Austria)

Supporting information for this article is available on the WWW under http://www.chemeurj.org/ or from the author. The following figures and data are available in addition: Diffuse reflectance UV/Vis spectra in the range 200–800 nm for all insertion compounds (1 figure), pre-edge fit data for both 77 K and 293 K XANES spectra (1 page), graphical illustration of the HgL_3 EXAFS fits at 77 K for all substances (3 figures), results of the EXAFS fits for $HgBr_2$ and HgI_2 insertion compounds at 300 K (1 page). See any current masthead page for ordering information.

  0947-6539/02/0817-3927 $ 20.00+.50/0

Introduction

The controlled and designed synthesis of novel host–guest compounds with new and unusual physical or chemical properties has become a highly desirable goal in recent solid state chemistry.[1] In such compounds, organisation on the molecular level is achieved by host–guest interactions which span the full range from weak van der Waals coupling to strong Coulomb interactions. With porous host matrices possessing a three-dimensional framework, the host topology remains nearly unchanged after the insertion of a guest, that is the structural response of the host to the guest component is small. For this reason, these host systems are well suited for the rational design of new host–guest compounds, as the structure of one component (the host) of the target composite is well-known and pre-determined. Design considerations can then focus on the geometrical fit between the pore system and the guest, and the tuning of host–guest interactions. The structural state of the guest species in these host–guest compounds can be either isolated (molecules/clusters in cage-like voids) or can possibly extend to one, two or three dimensions (when the host structure possesses channel-like voids) depending on the space offered by the host structure.

Among the host systems used, crystalline microporous host frameworks (zeotypes) have attracted much interest,[2–4] since they possess well-defined voids which are easily accessible for the guest components. Such frameworks typically have void sizes (channel or cage diameters) in the range 2.4–15 Å, allowing sufficiently small molecules to enter their voids, but ruling out the formation of bulk phases. Due to their intrinsic chemical, thermal and mechanical stability, framework structures relying on inorganic compositions (such as silica, aluminosilicate, aluminophosphate) are prime candidates for host structures. Many chemically different classes of molecules have been successfully introduced into such zeotypes, including organic,[5] organometallic[6, 7] and inorganic species,[4] resulting in composite materials with new properties. One of the most spectacular examples is the observation of second harmonic generation on the composite of *para*-nitroaniline in $AlPO_4$-5,[8] which does not occur in centrosymmetric bulk *para*-nitroaniline. The interest in such studies relies on the possibility of designing structures that are organised on the nanometer scale by regarding the microporous host framework as a negative template for the arrangement of the guest species. The concept of a pure templating function is realised when the host–guest interactions are very weak, apart from the geometrical exclusion of space occupied by the host framework. In this sense, the topochemical synthesis of zeotype composites by insertion of the guest species into porous frameworks may be considered as "structure-limited", compared to the "structure-directed" synthesis[9, 10] of the host structures themselves.

Often zeolites have been used as host compounds for the chemical constructions mentioned above. Zeolites feature an aluminosilicate framework, which is negatively charged; therefore, charge-compensating cations (e.g. Na^+, H^+) must be present. This leads to strong electrostatic coupling between the host framework and its guest species and in turn to considerable reactivity that is exploited in the typical applications of zeolites: ion-exchange, catalysis, adsorption. For assembling host–guest composites, this intracrystalline reactivity can be of advantage when molecules inserted into the voids react at the inner zeolite surface so that strong anchoring of the introduced species is achieved.[11] On the other hand, however, host–guest interactions then dominate the physical properties of the composites, and the design of composites by providing well-defined empty spaces within porous host compounds becomes very complicated when not only the geometrical arrangement of the guest species, but also their electronic states are influenced by their interactions with the host (or by interactions with the charge-compensating cations).

We have previously shown[12–17] that by the use of microporous silica modifications (so-called porosils)[18] instead of zeolites this problem can be eliminated. For example, the properties of iodine insertion compounds in various porosils are mainly determined by guest–guest interactions, which are in turn restricted by the available space in the porous host frameworks. Due to the electroneutrality (no charge-compensating cations necessary) and chemical inertness of the SiO_2 host, host–guest interactions are reduced to weak van der Waals forces.[12–17]

Here, we report the modular assembly of new host–guest compounds using porosils as rigid and inert host matrices and mercury(II) halides as the guest components.[17] Various porosils have been used, spanning the full range of pore dimensionalities from zero- to three-dimensional. The characteristic features of their structures are depicted in Figure 1,

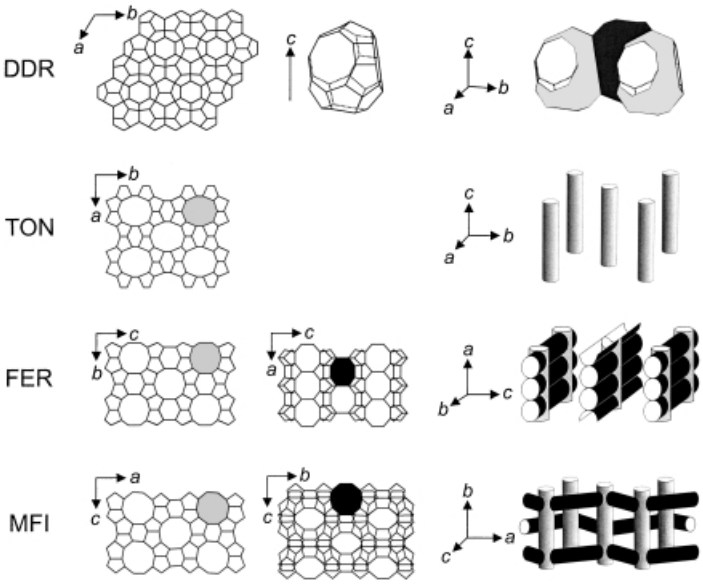

Figure 1. Zeosil host structures of the insertion compounds and of their pore systems (oxygen atoms are omitted for clarity).

and some structural data are summarised in Table 1. Decadodecasil 3R (short term: DDR)[19] possesses cage-like voids, thus representing the case of a quasi zero-dimensional host system. The cages are interconnected by means of eight-membered ring windows. In going from *silica*-theta-1 (TON) to *silica*-ferrierite (FER) and silicalite-1 (MFI), the pore

0947-6539/02/0817-3928 $ 20.00+.50/0 *Chem. Eur. J.* **2002**, *8*, No. 17

Table 1. Some structural data of the porosils used for the insertion of mercury(II) halides.

Porosil	DDR	TON	FER	MFI
pore dimensionality	$\left\{ \begin{matrix} 0 \\ \infty \end{matrix} \right\}$	$\left\{ \begin{matrix} 1 \\ \infty \end{matrix} \right\}$	$\left\{ \begin{matrix} 2 \\ \infty \end{matrix} \right\}$	$\left\{ \begin{matrix} 3 \\ \infty \end{matrix} \right\}$
free channel diameter [Å]	3.6×4.4	4.7×5.5	3.5×4.8 and 4.2×5.4	5.1×5.5 and 5.3×5.6
reference	[49]	[50]	[51]	[52]

dimensionality increases from one- to two- to three-dimensional. The idea behind the dimensionality concept is to possibly tune guest–guest interactions by restricting the geometrical arrangements of the guest species.[13] Besides dimensionality, the free space available within the pores is another important feature of the host systems. All framework structures used in this study possess 8- or 10-ring channels.[20] Hence, the space available for the guest molecules perpendicular to the channel axis is approximately the same for all porosils of higher pore dimensionality and is also comparable to the free diameter of the DDR cage. Therefore, the guest properties in hosts with different pore dimensionalities may be compared with each other.

The mercury(II) halides HgX_2 (with X = Cl, Br, I) form an interesting class of guest species. These substances form low-dimensional structures in the solid state (molecular crystals are formed by $HgCl_2$, $HgBr_2$ and the yellow modification of HgI_2, whereas red HgI_2 possesses a layered structure) and are readily volatised, so that the insertion or intercalation can be carried out easily by vapour transport. $HgCl_2$, for example, readily forms graphite intercalation compounds,[21] and $HgBr_2$ and HgI_2 have been intercalated into oxidic superconductors.[22]

Results

Compositions: In contrast to iodine insertion compounds of porosils, where the density of the guest molecules increases with host pore dimensionality,[13] no analogous trends regarding the composition can be found for the mercury halide insertion compounds (Table 2); however, some interesting facts can be recognised. For the DDR host, the loading decreases on going from $HgCl_2$ to HgI_2. The guest loadings indicate that in the case of $HgCl_2$, nearly every cage is occupied (5.87 out of 6 per 120 formula units SiO_2), whereas in the case of $HgBr_2$ and HgI_2 only approximately two thirds (3.95 out of 6) or one half (2.74 out of 6), respectively, of this value is obtained. These findings can be readily explained on the basis of purely geometrical considerations. The approximate lengths of the HgX_2 molecules along their molecular axes, as calculated from the interatomic distances and the van der Waals radii of the halogen atoms, are 8.2 ($HgCl_2$), 8.7 ($HgBr_2$) and 9.5 Å (HgI_2), respectively. The maximum free diameter between framework oxygen atoms at the top and bottom of the cages in the DDR structure with their ellipsoidal shape (Figure 1) is about 9.2 Å. Evidently, the small $HgCl_2$ molecule finds sufficient space within one cage and aligns itself to its long diameter, corresponding to the *c* axis of the host structure. Thus, each cage can be filled with one molecule. However, for the heavier mercury halide molecules this is not possible, since their van der Waals lengths are close to, or exceed, the free diameter of the DDR cages along the *c* axis, respectively. Correspondingly, under the condition that the molecules do not interact strongly with the host framework, that is that no contacts below the van der Waals distance occur, their arrangement must be different. Possibly, they are oriented with their long diameter within the *ab* plane, making use of the additional space provided by the 8-ring windows. Then, one $HgBr_2$ (or HgI_2) molecule may, with its center of mass (the Hg atom), be located either at the center of the 8-ring window or at the center of the cage, in the latter case with its halogen atoms protruding into neighbouring cage(s); either position rules out the occupation of all cages by one $HgBr_2$ or HgI_2 molecule. The different loadings of the DDR-based composites can thus be rationalised in terms of the increasing space requirements of the mercury halide molecules.

Another interesting feature of the composite stoichiometries is that the loading of the FER insertion compounds of HgX_2 are significantly lower than that of the corresponding iodine-loaded compound. For reference, the I_2-FER compound has a unit cell composition of $36\,SiO_2$:$3.2\,I_2$.[13] In the case of the mercury halides investigated here, the amount of guest species sorbed is clearly smaller (around 1.3 molecules per $36\,SiO_2$). This fact clearly illustrates the geometrical control of the host structure on the guest species. The FER structure consists of two types of channels, extended 10-ring channels and small 8-ring channels interconnecting them (Figure 1).[23] In the case of the iodine insertion compounds, both types of channels are filled, whereas in the HgX_2-FER samples, the inserted molecules probably only occupy the 10-ring channels.

Table 2. Compositions of HgX_2 insertion compounds.

Host	Unit cell composition (formula units/unit cell)			
	SiO_2	$HgCl_2$	$HgBr_2$	HgI_2
DDR	120	5.87	3.95	2.74
TON	24	1.41	1.35	0.62
FER	36	1.38	1.37	1.16
MFI	96	6.14	6.15	5.92

Electronic spectra: The UV/Vis spectra of HgX_2 molecules are dominated by strong absorptions arising from dipole-allowed electronic transitions from the $^1\Sigma_g^+$ ground state to the $^1\Pi_u$ and $^1\Sigma_u^+$ states.[24] For the $HgCl_2$- and $HgBr_2$-loaded samples, only the former transition was detected within the instrumental wavelength range, for HgI_2 composites both transitions were observed (see Figure 2 for some representative examples). Generally, the broad bands ($^1\Pi_u \rightarrow {}^1\Sigma_g^+$) peak in the range of 200–207 nm for inserted $HgCl_2$ and 228–235 nm for inserted $HgBr_2$. The two resolved peaks for the HgI_2 insertion compounds have their maxima between 210 and 218 nm ($^1{}_u \rightarrow {}^1\Sigma_g^+$) and 273 and 285 nm ($^1\Sigma_u^+ \rightarrow {}^1\Sigma_g^+$), respectively. The spectra resemble those of the molecules in the vapour phases of the halides[25] and those of mercury

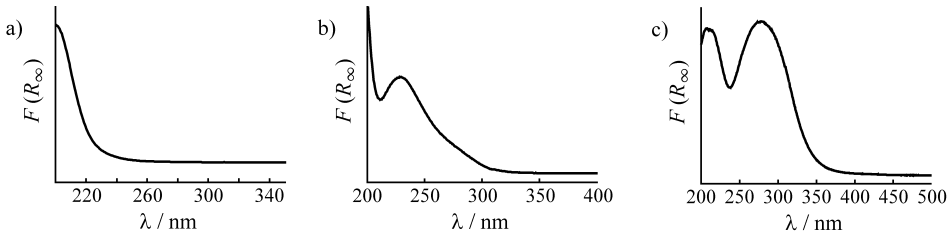

Figure 2. Representative UV/Vis spectra (represented by their Kubelka-Munk functions) of mercury(II) halides inserted in DDR: a) $HgCl_2$–DDR, b) $HgBr_2$–DDR, c) HgI_2–DDR. Spectra for the same inserted mercury halides in different host systems are very similar.

halides in weakly interacting solvents.[26] There is no evidence for clustered $(HgX_2)_n$ species, as was obtained for HgX_2 insertion compounds of zeolites.[27]

X-Ray absorption spectroscopy: *XANES*: The discussion of the XANES spectra begins with the spectra of the bulk mercury halides (Figure 3). Two features, labeled *A* and *B* in Figure 3, can be discerned on the rising edge of the HgL_3 XANES spectra of $HgCl_2$ and $HgBr_2$. In ref. 28, similar

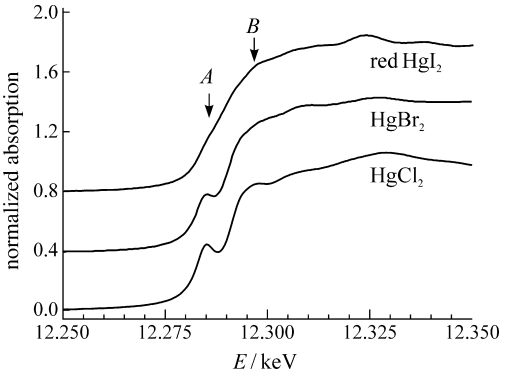

Figure 3. HgL_3 XANES spectra of bulk mercury halides (measured at 77 K). The pre-edge feature *A* and the main-edge feature *B* are denoted by arrows. Spectra are offset vertically for clarity.

features were observed in solutions containing HgX_2 molecules. These authors assigned them to the dipole-allowed transitions $2p_{3/2} \rightarrow 6s$ and $2p_{3/2} \rightarrow 6d$.[29] Whereas peak *A* is clearly seen in the spectra of solid $HgCl_2$ and $HgBr_2$, peak *B* is broader, possibly due to intermolecular interactions in the solid state (even when bulk $HgCl_2$ and $HgBr_2$ must be considered as "molecular" solids composed of linear molecules, there are additional intermolecular Hg–X interactions, resulting in 2+4 coordination). This effect becomes considerably stronger for red HgI_2, where only a very weak transition in the region of peak *A* and no significant peaking of the absorption in the region of feature *B* is observed. Red HgI_2 is a (wide band-gap) semiconductor with a pronounced band structure,[30] and electronic transitions to empty bands (as compared to empty molecular orbitals) are expected to be significantly broadened, explaining the damped intensity of peak *A* and the absence of further distinct features in the XANES of red HgI_2.

Turning this argument around, a sharpening of XANES peaks corresponding to electronic transitions can be taken as a signature of reduced interactions between molecules. This is observed for the peak *B* on going from the pure halides to the insertion compounds of $HgCl_2$ and $HgBr_2$ (Figure 4). It has also been reported that the pre-edge peak *A* sensitively reflects the local surrounding of Hg in mercury(II) compounds and that its intensity strongly depends on the coordination geometry, for example linear, trigonal planar or octahedral.[31] The intensities and the shapes of this peak are very similar for the pure halides and for the insertion compounds of $HgCl_2$ and $HgBr_2$ (see Supporting Information), indicating that the local geometry around the Hg-absorber atom remains linear in the insertion compounds with no evidence for additional coordination from the porosil framework. Turning to the HgI_2 insertion compounds, the sharpening of the features *A* and *B* is even more pronounced. This can be rationalised on the basis that the electronic structure changes from a semiconductor band structure[30] to a molecular orbital picture, with the discrete final states of the inserted molecules giving rise to sharper transitions. Quantitative data analysis by least-squares fitting of the peaks *A* and *B* for the spectra measured at 77 and 293 K indicates that the intensities and the widths are similar (see Supporting Information). Therefore, neither at room temperature nor at the lower temperatures examined here, is there evidence for additional coordination of the guest molecules by the SiO_2 framework.[32]

For $HgBr_2$-containing compounds, spectra at the Br*K* edge were recorded, too. An analysis of their pre-edge peaks, which are assigned to $1s \rightarrow 4p$ transitions, deserves special attention due to the fact that the white-line intensity has been shown to change with the electron transfer from the host lattice in the case of oxidic superconductors.[22c] For the $HgBr_2$–porosil composites, however, the pre-edge peaks remain essentially unchanged upon insertion. Therefore, the investigations on the Br*K* edge demonstrate that no electron transfer occurs between the SiO_2 framework and the inserted $HgBr_2$ molecules, another indication of the weakness of the interactions between host and guest.

Within each series of spectra, the multiple scattering features appearing at energies above the edge are quite similar (except for that of bulk HgI_2), again indicating a similar local environment of the Hg atoms. This is in line with the assumption that in all cases monomeric linear HgX_2 molecules are present.

EXAFS: As typical examples of the results from HgL_3 EXAFS measurements, the Fourier transforms (*FT*s) of HgX_2–DDR composites are presented in Figure 5 (see Supporting Information for more analyzed EXAFS spectra). The first peaks in the *FT*s correspond to the halogen atoms neighboring the mercury atoms. The back-transformed EXAFS oscillation corresponding to this coordination shell is also shown in Figure 5. The results of a quantitative analysis obtained by fitting the EXAFS oscillations of the back-transforms of the first peak in the *FT*s are summarised in

  0947-6539/02/0817-3930 $ 20.00+.50/0 *Chem. Eur. J.* **2002**, *8*, No. 17

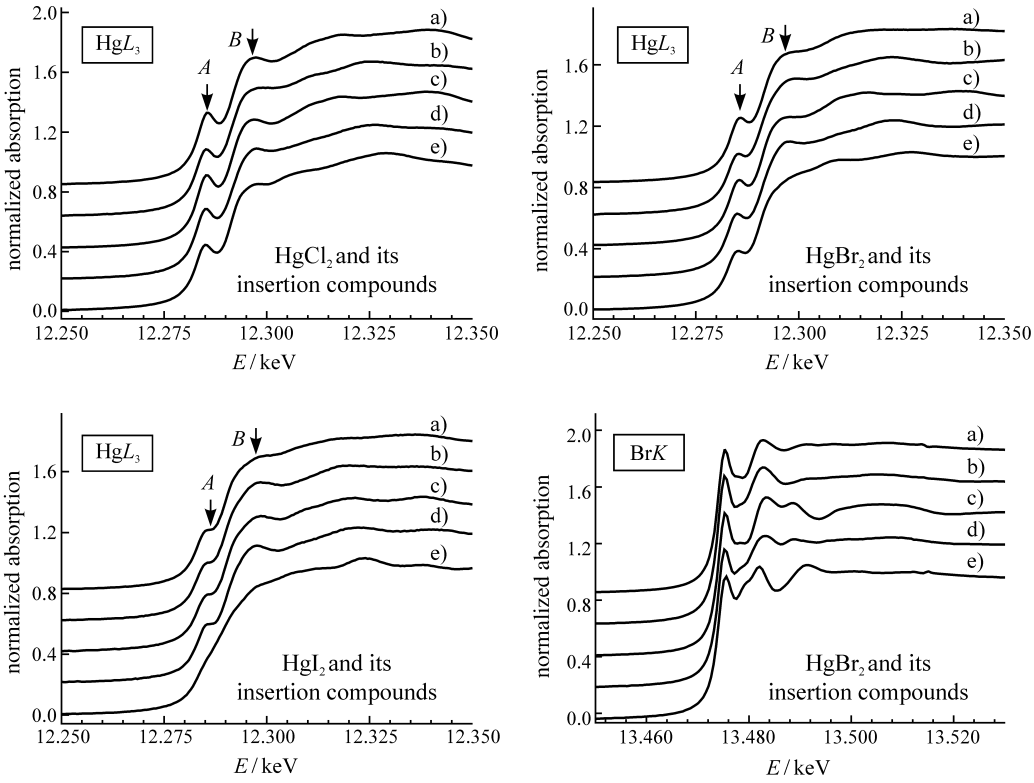

Figure 4. HgL_3 and BrK XANES spectra of HgX_2-porosil insertion compounds in comparison to the spectra of the bulk mercury halides (spectra measured at 77 K): a) HgX_2–MFI composites, b) HgX_2–FER composites, c) HgX_2–TON composites, d) HgX_2–DDR composites and e) bulk mercury halides. The pre-edge feature A and the main-edge feature B are denoted by arrows. Spectra are offset vertically for clarity.

Table 3 for all insertion compounds and for the bulk HgX_2 solids (bond lengths of the HgX_2 molecules in the vapour phase are also given). The data given here refer to measurements at 77 K; results derived from measurements at 293 K are very similar (except for larger σ^2 values), indicating that no substantial differences appear in the local environments of the inserted HgX_2 molecules within this temperature range. From the BrK spectra of the $HgBr_2$ insertion compounds, a similar procedure yields Br–Hg distances between 2.36 and 2.38 Å, in good agreement with the data resulting from the analysis of the HgL_3 EXAFS oscillations of these compounds (Table 3).

Table 3. Results of EXAFS analysis of HgL_3 spectra recorded at 77 K. Coordination numbers for Hg were set to two (except for red HgI_2 where it was four). σ^2 denotes the Debye–Waller-type factor and S_0^2 the amplitude reduction factor; R is a measure for the difference between the experimental data and the fit. Hg–X distances are accurate to ± 0.02 Å. Bond distances of the HgX_2 molecules in the vapour phase[33] and for solid yellow HgI_2 (which was not investigated experimentally) are given for comparison.

Compound	Hg–X distance [Å]	$10^3 \times \sigma^2$ [Å^2]	ΔE_0 [eV]	S_0^2	R
$HgCl_2$ (vapour)	2.250				
$HgCl_2$–DDR	2.275	2.4	1.3	1.15	8.9
$HgCl_2$–TON	2.263	2.2	0.9	1.18	11.4
$HgCl_2$–FER	2.272	2.4	0.1	1.16	11.1
$HgCl_2$–MFI	2.261	2.0	0.7	1.11	9.0
$HgCl_2$ (solid)	2.290	2.3	1	1.15	11.8
$HgBr_2$ (vapour)	2.374				
$HgBr_2$–DDR	2.397	2.1	0.1	1.13	11.3
$HgBr_2$–TON	2.389	2.2	0.2	1.17	11.2
$HgBr_2$–FER	2.398	2.2	1.8	1.07	14.9
$HgBr_2$–MFI	2.397	2.4	0.1	1.13	14.2
$HgBr_2$ (solid)	2.459	2.7	1.2	1.18	12.3
HgI_2 (vapour)	2.553				
HgI_2–DDR	2.569	1.7	0.2	0.97	16.1
HgI_2–TON	2.575	2.0	1.6	1.24	13.9
HgI_2–FER	2.573	1.6	1.8	0.99	12.7
HgI_2–MFI	2.571	1.8	0.1	1.05	11.8
HgI_2 (solid, red)	2.786	4.2	0.5	1.05	15.9
HgI_2 (solid, yellow)	2.615				

For all insertion compounds, the Hg–X bond lengths of the occluded HgX_2 molecules are very near to those of the corresponding molecules in the vapour phase[33] and are the shortest observed in the solid state so far (with one exception: in an isolated HgI_2 molecule in the structure of $[Cu(2\text{-pyrazinecarboxylato})_2HgI_2]\cdot HgI_2$ a Hg–I distance of similar length is found, d(Hg–I) = 2.577(2) Å).[34] Especially, for the inserted $HgBr_2$ and HgI_2 molecules, these distances are significantly shorter than those of the solid-state structures of the pure halides (Table 3). Thus, for the insertion compounds of $HgBr_2$ and HgI_2, the EXAFS results provide clear evidence that, in spite of the solid nature of the compounds, the geometry of the occluded molecules is very similar to those of the corresponding molecules in the vapour phase, showing the weakness of the interactions of the molecules with their surrounding; in the case of $HgCl_2$, all Hg–Cl bond lengths are within a small range (see Table 3) so that a similar conclusion cannot be drawn from these data. However, it will be shown below that also in these compounds, only very weak host–guest and guest–guest interactions exist.

It is worth noting that the HgL_3 EXAFS provides no evidence for Hg–O contacts in the range of the expected van

  0947-6539/02/0817-3931 $ 20.00+.50/0

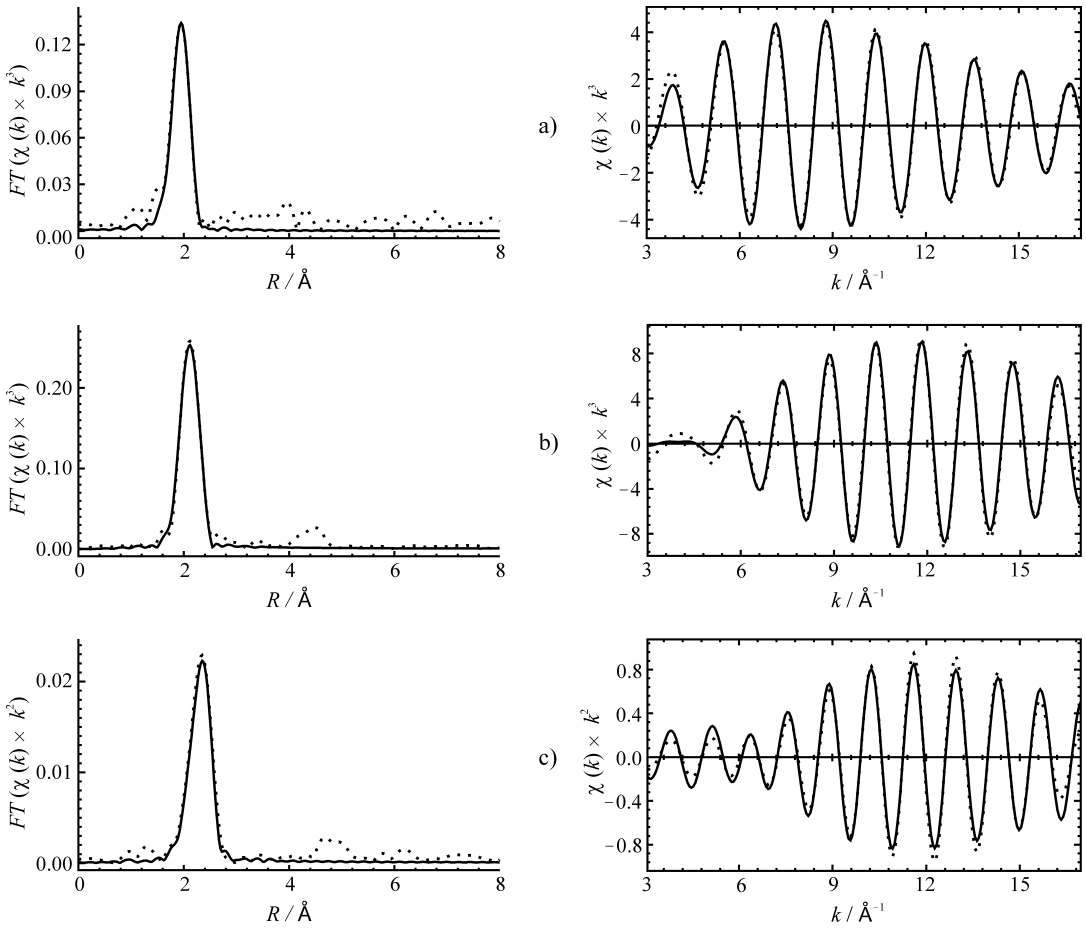

Figure 5. Evaluation of the HgL_3 EXAFS (measured at 77 K) of HgX_2 molecules inserted into the DDR host matrix: a) $HgCl_2$–DDR, b) $HgBr_2$–DDR, c) HgI_2–DDR; left: Fourier transforms of the EXAFS data (dotted lines), right: single-shell EXAFS derived by the back-transformation of the peaks corresponding to the first coordination shell (dotted lines); fits to these data (full lines) are shown in real space (to the *FT*s on the left side) and in *k* space (to the single-shell EXAFS data on the right side). Distances on the *R* scale of the *FT*s are not corrected for phase shifts.

der Waals distance of around 2.6 Å. This is most probably due to the variability of host–guest contacts that can be realised between the framework and the inserted molecules due to the possibility of guest molecules occupying many different positions within the voids. This leads to smearing out of the back-scattering signal from the oxygen atoms. This corresponds to a strong disorder in the host–guest relationship, whereas the disorder within the inserted molecules is very small. This is shown by a consideration of the Debye–Waller factors σ^2, which consist of two contributions, a vibrational one and one due to static disorder.[35] The σ^2 values of the inserted molecules are comparable to those of the bulk halides for $HgCl_2$ and $HgBr_2$, implying that the static disorder within the inserted molecules is very small. For HgI_2, the σ^2 of the inserted molecules are lowered relative to the bulk, a fact which is explained by the lower coordination number (two versus four) and the reduced bond lengths for the occluded molecules, corresponding to a higher strength of the intramolecular bonds and resulting in turn in a large reduction of the vibrational contribution to σ^2.

All *FT*s of EXAFS oscillations, those derived from the HgL_3 as well as those derived from the Br*K* spectra, show additional peaks between 3.5 and 5 Å (see, for example, Figure 5 and the Supporting Information). A detailed analysis shows that these peaks are neither due to backscattering from the host pore walls nor to backscattering from other guest molecules, but stem from intramolecular multiple scattering,[36] which is pronounced due to the linear geometry of the inserted molecules (focussing effect).[35]

Raman spectroscopy: Whereas UV/Vis and XANES probe the energy difference between the electronic ground state and excited states, Raman spectroscopy is sensitive to changes in the vibrational spacings within the ground state. Previous extensive investigations by Perrson et al. have shown the vibrational frequencies of HgX_2 molecules in different solvents strongly depend on the interaction with the surroundings.[37] An important conclusion which can be drawn from this work is that increasing solute-solvent interactions lead to a red-shift of the Raman-active ν_3 mode (as compared to the vapour phase). Furthermore, the deviation from a linear $D_{\infty h}$ geometry to a bent C_{2v} geometry seems to go hand in hand with increasing solute-solvent interaction.

For the mercury halide molecules in the various porosil hosts used in this study, the frequencies of the Raman bands are found to be only slightly red-shifted in comparison to the vapour-phase values (Table 4); for occluded $HgCl_2$, the frequencies are similar to those observed on these molecules

  0947-6539/02/0817-3932 $ 20.00+.50/0 *Chem. Eur. J.* **2002**, *8*, No. 17

Table 4. Frequencies of the ν_3 mode (cm^{-1}) for HgX_2 molecules occluded in porosils (measured at 298 K) in comparison to those of the solid phase (measured around 500 K),[53] those of the vapour phase (measured at 728 K)[33] and those dissolved in furan (298 K).[37]

Sample	Pure solid	Liquid	Vapour	Solution	DDR	TON	MFI
$HgCl_2$	311	311	355	339	338	341	341
$HgBr_2$	187	197	220	212	212	216	216
HgI_2	137	142	157	155	156	158	157

in weakly coordinating solvents like furan and benzene.[37] For HgI_2 molecules, the frequencies are very similar for the gaseous, the dissolved and the inserted state. For mercury bromide, the situation is intermediate. These findings are a strong expression of the fact that the inserted molecules are nearly unperturbed when compared to the isolated state in the vapour phase and thus the host–guest interactions in these compounds are very weak.

There appears to exist a tendency for the frequencies observed for HgX_2 in the pore systems with higher dimensionality (TON, MFI) to be higher than those observed on the DDR host (Table 4); they are thus even nearer to the vapour-phase values. These differences might reflect a slightly increased interaction between the host framework and the guest species in the case of the DDR insertion compounds with their narrow cages.

A further interesting aspect of Raman spectroscopy is that this spectroscopic technique can reveal information about the species isolated after the simultaneous insertion of two mercury halides. Starting the insertion process from an equimolar mixture of two halides HgX_2 and HgY_2 (for example, $HgBr_2$ and HgI_2), the spectra of the insertion compounds show bands which correspond to the pure HgX_2 and HgY_2 molecules as well as the mixed halides HgXY. After the incorporation into the porosils, the mixed mercury(II) halides are stable and do not decompose into the simple HgX_2 and HgY_2 molecules when stored under ambient conditions as the pristine mixed halide molecules do.

IR spectroscopy should, in principle, be able to corroborate the results found by Raman spectroscopy. Moreover, indications with regard to the X-Hg-X bond angles could possibly be obtained. However, in the IR spectra the wavelength range of interest is covered by very broad absorptions due to the silica host structures. Unfortunately, it was thus impossible to detect any vibrations that could be assigned to the guest molecules.

Raman microscopy: Another interesting aspect of these novel host–guest compounds can be elucidated by polarised microscopic Raman spectroscopy. Regarding the close fit between the van der Waals diameters of the guest molecules and the free pore space available, one can expect an alignment of the guest species. By measuring the Raman intensity of an individual crystal along different crystallographic directions, an alignment of the molecule under investigation should result in a strong directional dependence of the scattered Raman intensity. Here, we show a corresponding experiment for $HgBr_2$ molecules embedded in the TON host structure (this one-dimensional host structure is expected to show the clearest orienting effect). Typical Raman spectra obtained in different polarization directions for the incoming laser light and the outgoing scattered light are depicted in Figure 6. The dependence of the spectra on the polarization clearly reveals that the HgX_2 molecules inside the one-dimensional channels of this host structure are aligned with their molecular axis close to the *c* axis of the host structure, which is parallel to the

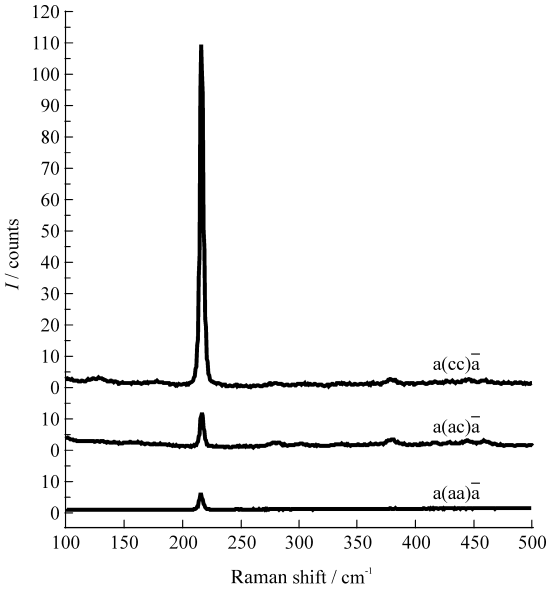

Figure 6. Microscopic Raman spectra (298 K) of $HgBr_2$ embedded in the TON host structure for different polarization directions of the incoming laser light and the scattered radiation, respectively. Spectra are designated in terms of the crystal axes. The nomenclature for the polarization of the light and the orientation of the crystal corresponds to that used in ref. 54.

channel direction. Hence, the host matrix is able to induce orientational order of the guest molecules although, as proved by the results above, the host–guest interaction is weak. Unfortunately, the host crystals are always twinned and in addition, they are relatively small. Although these facts make the construction of an exact model for the orientational distribution of the guest molecules impossible, the alignment can be evaluated using some simplifications. These studies will be reported in detail elsewhere.[38]

Discussion

From the results given in the preceding section, it can be concluded that only very weak interactions exist between the inserted mercury halide molecules and the surrounding crystalline $[SiO_{4/2}]$ framework. It is these interactions which are responsible for the formation of the insertion compound during its production. With respect to the insertion reaction, kinetic considerations also have to be taken into account since it might be argued that the insertion process is in fact a kinetic trapping of guest molecules during cooling to room temperature after the insertion reaction has taken place. However, in this study the cooling times from around 450 K down to room temperature were as long as 10 h. Also, the reaction times necessary to achieve a reproducible full loading were long (12 h). Furthermore, applying the same reaction conditions to

single crystals with dimensions on the millimeter scale and to finely powdered samples results in the same degree of loading. All these facts show that the compounds obtained correspond to the products of thermodynamic equilibria and that they do not result from a kinetically controlled trapping process.

Evidently, the strength of the host–guest interactions in the HgX_2–porosil compounds is finely balanced. Although the host–guest interactions are sufficiently strong as to drive the formation of the insertion compounds, they are weak enough to leave the molecules nearly unperturbed. The physical data relating to their electronic (UV/Vis, XANES) and geometric (EXAFS, Raman spectroscopy) structure resemble those of the corresponding molecules in the gas phase or in solutions with non-coordinating solvents.

With respect to the special nature of the host–guest compounds under study, it is not surprising that all attempts to perform X-ray structural analyses, either on single crystals (DDR-, FER- and MFI-based insertion compounds) or on powders (TON-based insertion compounds) failed. Evidently, the guest molecules do not occupy well-defined, translationally equivalent positions within the voids of the host, but are strongly disordered. Due to the high X-ray scattering factors of the guest molecules, the intensities of the X-ray diffraction peaks are dominated by disordered components, rendering structural analysis very difficult or impossible. In any case, the local spectroscopic techniques applied in our work yield more information about the guest species than could possibly be obtained by X-ray structural analyses of such strongly disordered systems.

With regard to the special nature of the host–guest compounds studied here, it is also of interest to compare the porosil insertion compounds with HgX_2 complexes of crown ethers and short-chain oligoethylene glycols. In those compounds, there are clear indications of coordination of the Hg atom by the oxygen atoms of the complexing ligand.[39] However, these coordinations are weak as manifested by the large Hg–O distances of at least 2.66 Å, near to the sum of the van der Waals radii. Nevertheless, the intramolecular Hg–X distances in such compounds are in all cases slightly enlarged when compared to the vapour phase values: 2.29, 2.40 and 2.60 Å, respectively, for crown ether complexes of $HgCl_2$, $HgBr_2$ and HgI_2. (We note in passing that the elongation is much more pronounced when there are stronger interactions between HgX_2 molecules and their surrounding, for example $d(\mathrm{Hg{-}Cl) = 2.34}$ Å in the graphite intercalation compound of $HgCl_2$,[21b] $d(\mathrm{Hg{-}I) = 2.645}$ Å in HgI_2-intercalated bismuth-containing oxidic superconductors[22d]). Also, the HgX_2 units often have a slightly bent geometry in these complexes. Both these facts are clear indications of a true coordination by O atoms. These findings, obtained from single-crystal X-ray structural analysis, have no equivalents in the results obtained on the porosil insertion compound by spectroscopic methods. Neither are the Hg–X bond lengths enlarged, nor are there any indications that deviations from the linear structure occur. Thus, although the $[SiO_{4/2}]$ framework of a porosil might be considered as a "macroligand" with oxygen donor atoms, and in this sense might be considered to bear some similarities to crown ethers, there are clear differences. First, the coordinating ability of the siloxane oxygen atoms is expected to be lower than that of oxygen atoms of ether linkages. Probably more importantly, the siloxane oxygen atoms are incorporated into a three-dimensional framework, and the development of an optimal coordination is hindered by its rigidity. This stands in contrast to the case of HgX_2-crown ether complexes, where the "crown" may become appreciably flattened due to the coordination.[39] The SiO_2 framework with its restricted coordination ability thus rather behaves like a weakly coordinating solvent, which is in agreement with the experimental findings. This property of the framework makes insertion compounds of porosils interesting systems for a novel type of matrix-isolation study; such systems are stable from very low up to the desorption temperatures (typically some 100 °C above room temperature) and possess a well-defined, three-dimensional periodical "solvent" matrix, properties which contrast strongly with the classical low-temperature amorphous noble-gas matrices. For example, the dynamics of iodine dissociation within the cages of the DDR structure have been investigated by femtosecond time-resolved spectroscopy at room temperature.[40] The interpretation of the results from these experiments was simplified greatly by the exact knowledge of the structural surroundings of the guest molecules. In this context, it is also worth pointing out that this type of matrix isolation is not limited to small molecules; larger well-defined molecules (such as S_7, Se_6) can also be occluded in microporous SiO_2 modifications.[14, 16] In addition, the high optical transparency of silica makes other tempting experiments possible. After the insertion of photolabile precursors to reactive molecules into the voids, such reactive species could be produced in the crystalline matrix by irradiation with light.

There is of course a second factor which is responsible for the truly isolated physical state of the HgX_2 molecules inside these solid matrices. Not only are host–guest interactions weak, but also interactions between guest molecules are virtually absent. This contrasts with the behaviour of the analogous iodine insertion compounds, where a weak coupling between the guest molecules is present. This coupling can be engineered by the pore dimensionality of the host to give isolated I_2 molecules (iodine–DDR) or one- and three-dimensionally (iodine–TON and iodine–MFI, respectively) interacting entities.[12, 13] There is no evidence for such intermolecular interactions between the HgX_2 guest molecules in the porosils, although in the pure solids of the mercury halides such interactions are present, as shown by the additional coordination of the Hg atoms by X atoms in the molecular structures of $HgCl_2$, $HgBr_2$ and yellow HgI_2 (resulting in a 2+4 coordination), by the structure of red HgI_2 (with a coordination number of four for the Hg atom) and by the fact that the Hg–X distances in these solids are enlarged as compared to the distances in the vapour phase. When considering the (2+4) distorted octahedra (as an excerpt from the solid-state structures) or the dimer molecules Hg_2X_4 (with structures taken from a high-level computational study),[41] as models for interacting HgX_2 molecules, it becomes clear that geometric restrictions prevent any intermolecular interactions in the voids of the porosils, as none of these entities fits into the pores of the host frameworks.

  0947-6539/02/0817-3934 $ 20.00+.50/0 *Chem. Eur. J.* **2002**, *8*, No. 17

Hence, it is clear that it is the small size of the pores which is responsible for the observation that the properties of the inserted mercury halides do not show any dependence upon the host pore dimensionality. Porosils with larger pore openings (for example UTD-1)[42] might allow such interactions and could thus provide the opportunity to selectively tune the guest–guest interactions by the host-pore dimensionality and hence the electronic properties of the guest species.

The restricted space provided by the host pore structure not only prohibits guest–guest interactions, it also causes a geometrical alignment of the guest molecules. At a first glance, this result might seem surprising and counter-intuitive to the argument that host–guest interactions are weak as discussed above. However, the alignment does not result from electronic interactions, but is due only to the close fit between the host pore systems and the guest molecules, leading to a strong geometric restriction of the orientational freedom of the guest molecules. In our Raman spectroscopic studies, we have not found any evidence for liberation of the HgX_2 molecules inside the cages or channels of the porosils, in contrast to the case of iodine molecules in their corresponding insertion compounds.[15] Hence, for the host structures containing channels, the arrangement of the guest molecules can best be understood as a disordered one-dimensional sequence of non-interacting HgX_2 molecules, which can only be slightly tilted against the channel axis. This type of arrangement is corroborated by the strong polarization dependence of the Raman spectra of HgX_2 molecules in TON.

Such new inorganic–inorganic hybrid materials with unusual physical properties of the guest molecules may find applications in systems that can otherwise only be constructed using the vapour phase. For example, gaseous mercury(II) halides can be used to achieve lasing over a wide spectral range, based on the photodissociation of HgX_2 molecules.[43] However, the need for elevated temperatures to obtain a vapour phase of high density as well as the corrosive nature and toxicity of the pure halides constitute major problems. After the occlusion in porosils, however, these disadvantages are eliminated while a vapour phase-like state is preserved. Thus, the composite materials described here could in principle act as solid-state laser media. Unfortunately, preliminiary investigations in this direction have shown the fluorescence of the occluded molecules to be strongly quenched by the host framework,[44] an effect which might be overcome by the use of other laser-active guest molecules (such as noble gas atoms) or with other electroneutral microporous hosts like some members of the $AlPO_4$ family. In addition, high laser powers cause desorption of the occluded halides (see Experimental Section, Raman spectra).

Conclusion

The concept of using the well-defined, three-dimensional regularly arranged pore systems of crystalline microporous SiO_2 frameworks as templates for the arrangement of guest molecules offers a new synthetic route to host–guest compounds with very weak host–guest interactions and strongly reduced guest–guest interactions.[12–17] By choosing the appropriate pore systems (from among the ca. 35 porosil topologies known), the designing of a specific assembly of host–guest systems becomes possible. Hence, on the basis of simple geometrical considerations only, the synthesis of solids can be planned and the interaction between the guest species can be tuned. The approach is simple, as the porosil hosts can be obtained in their porous forms by structure-directed hydrothermal synthesis and calcination. A further advantage of these hosts with regard to the subsequent vapour-phase insertion is their high temperature stability, which allows the loading to occur at temperatures as high as 1100 K, where many elements and compounds possess a sufficiently high vapour pressure.

Judging the quality of design of solid-state compounds with regard to the present study, we note that the insertion compounds of mercury halides present an extreme case where guest–guest interactions are excluded. This is clearly due to the strong geometrical confinement imposed by the host structures. As host–guest interactions are very weak, too, supramolecular assemblies are obtained where the guest species exhibit quite unusual physicochemical properties. The isolated HgX_2 molecules in the insertion compounds resemble those present in the gas phase or those dissolved in non-coordinating solvents, so that the host frameworks can be considered as "solid solvents" which do not coordinate strongly to the guest molecules. In addition, the geometric restrictions imposed by the crystalline host structure can induce orientational ordering by a templating effect. Summarizing these unusual properties, the HgX_2 "sub-phase" in the insertion compounds could be considered as a "structured and oriented gas", a very unusual state of matter.

These substances are attractive for applications where high densities of non-interacting, but ordered molecules are necessary. Optical applications, as an example, profit from the high transparency of the silica host framework in the NIR to UV range. There are also interesting opportunities for spectroscopic matrix-isolation studies, with the advantage that the matrix structure is known exactly and that the compounds possess a wide range of thermal stability, allowing spectroscopic experiments to be performed between the lowest temperature experimentally available and the desorption temperature of the inorganic guest molecules.

Experimental Section

Synthesis

Host materials: 1-Aminoadamantane, 1,6-diaminohexane, pyridine/propylamine and tetrapropylammonium were used as structure-directed agents to induce the formation of DDR, TON, FER and MFI, respectively. The hydrothermal syntheses of the host compounds TON, FER and MFI were performed according to established literature procedures;[45] the synthesis of DDR is described in detail in reference [13]. To remove the molecules of the structure-directing agents occluded in the material after synthesis, the samples were calcinated. For that purpose, about 1 g of the sample was placed in an Al_2O_3 crucible and positioned in the center of a conventional oven. All calcination experiments were carried out in air. The heating programs were optimised to ensure complete combustion of the organic matter while maintaining a high crystallinity of the host material. Suitable temperature profiles for the different host materials are: DDR: 293 → 1123 K within 10 h, hold for 4 h, 1123 → 293 K within 24 h; TON: 293 →

1123 K within 48 h, hold for 84 h, 1123 → 293 K within 24 h; FER: 293 → 1093 K within 84 h, hold for 84 h, 1093 → 293 K within 24 h; MFI: 293 → 623 K within 10 h, hold for 12 h, 623 → 6773 K within 8 h, hold for 24 h, 773 → 873 K within 8 h, hold for 40 h, 773 → 923 K within 8 h, hold for 48 h, 923 → 293 K within 24 h. These calcination programs are suitable for both powdered samples and single crystals with dimensions of up to 1 mm. After calcination the products were colorless, as were the as-synthesised materials. X-ray powder patterns confirmed the integrity of the host structures after calcination; no peaks due to dense SiO_2 modifications (such as cristobalite) were detected. In addition, single crystals did not show any cracks under an optical microscope.

Insertion: The insertion of the guest molecules was realised by deposition in the gas phase in evacuated and closed quartz tubes. The tubes were placed in an oven, with the host compounds held at the upper end of the tubes by quartz wool and the guest compounds placed at the bottom. This setup avoids condensation of bulk guest material on the host surface during cooling. Typically, 0.2 g host material and 0.6 g to 1.0 g of a mercury halide (1.0 g of equimolar mixtures of two mercury halides in the case of HgXY insertion reactions) were used in an insertion experiment. Insertion temperatures were chosen according to the volatility of the guest compound: $HgCl_2$: 633, $HgBr_2$: 643, HgI_2: 653 K. Before sealing, the open quartz tubes containing the host only were dried at 423 K in a forced air oven. Although porosils are, in principle, hydrophobic in character, it turned out that without this step the inserted samples in all cases become dark grey. This is most probably due to remaining water traces which cause reduction of the mercury(II) halides during the insertion reaction. The quartz tubes were held at the insertion temperatures for 12 h and then slowly cooled down to room temperature within 10 h. Slight deviations in the insertion temperature or longer insertion times did not affect the amount of guest molecules introduced.

Basic characterization: The guest contents were determined by thermogravimetry on a Mettler TA2 thermogravimetric balance under a flow of argon (5 $L\,h^{-1}$) with a heating rate of 10 $K\,min^{-1}$ with the sample held in a corundum crucible. Measurements on single crystals and on powders show the guest contents to be the same in both cases. Hence, we assume that the amount of mercury halides adsorbed on the surface of the porosil particles is negligible. X-ray powder diffraction patterns of as-synthesised, calcined and loaded hosts, respectively, were recorded at room temperature with $Cu_{K\alpha}$ radiation on a Philips 1710 Bragg-Brentano diffractometer equipped with a graphite secondary monochromator.

XAFS spectroscopy: HgL_2-, HgL_3- and BrK-edge spectra were recorded at HASYLAB/DESY in Hamburg (Germany). The storage ring DORIS III was operated at 4.432 GeV with an injection current of 100 mA. The data were collected at beamline X1.1 at room temperature and at 77 K in transmission mode by monitoring the X-ray intensities with ionization chambers. The spectrometer is equipped with a Si(311) double-crystal monochromator. For energy calibration, the WL_1 edge of $CaWO_4$ was recorded simultaneously with each of the HgL_3 edge samples, whereas for the HgL_2 edge and the BrK edge samples the BiL_3 edge of a Bi foil was simultaneously recorded. In all experiments, detuning of the monochromator to 50% of the maximum intensity served to reduce contributions of higher harmonics to the X-ray beam. For the measurements, carefully ground powders were pressed into polyethylene pellets (Merck, spectroscopic grade). The amount of sample was adjusted to give edge jumps $\Delta\mu d$ of 0.3 – 0.8. The spectra were processed using the program WinXAS.[46] For energy calibration of the HgL_3 edge spectra, the first inflection point of the WL_1 edge was set to a value of 12.100 keV. This corresponds to a value of 11.103 keV for the first inflection point at the GeK edge of a Ge foil.[47] For the calibration of the HgL_2 edge and the BrK edge spectra, the first inflection point at the BiL_3 edge of the Bi foil was set to 13.419 keV.[47] The background of the sample spectra was modeled using Victoreen-type functions; it was subtracted from the experimental curves. The edge jump $\Delta\mu d$ was then set to an absorption value of 1 to be able to compare the XANES spectra. EXAFS analysis of HgL edge and BrK edge spectra was performed according to standard procedures.[35] After conversion of the normalised spectra into k space, the EXAFS oscillations were extracted by modeling the non-oscillatory part of the spectra with cubic splines which were then subtracted from the spectra. Weighting factors applied on the EXAFS curves were: HgL_3 edge spectra: k^3 for $HgCl_2$ and $HgBr_2$ compounds, k^2 for HgI_2 compounds; BrK edge spectra: k^2. HgL_3 EXAFS data were Fourier-transformed in the range from $k = 3 - 17$ $Å^{-1}$; BrK EXAFS data were Fourier-transformed in the range from $k = 3 - 17$ $Å^{-1}$. From the Fourier transforms, the first peaks corresponding to the nearest neighbour atoms were back-transformed to obtain the single-shell EXAFS. Phase and amplitude functions were then calculated for the HgX_2 molecules in their gas phase geometries with the program FEFF 7.02.[48] To obtain the structural parameters (interatomic distance Hg–X and Debye – Waller-type factor σ^2; the coordination number was fixed at two in the case of HgL_3 EXAFS data and to one in the case of BrK EXAFS data), the back-transformed single-shell EXAFS data were fitted in the range from $k = 3 - 17$ $Å^{-1}$ using these functions.

UV/Vis spectroscopy: UV/Vis spectra were obtained in diffuse reflectance on a Cary 5 (Varian) spectrometer equipped with a Praying Mantis device at room temperature. The calcined host materials served as references. For each host – guest compound, several spectra were recorded, with the specimen diluted by varying amounts of the host compound; no influence of the dilution by the host compound was recognised. Hence, the Kubelka – Munk function was considered to be representative of the absorption spectra and was applied to the data.

Raman spectroscopy: Raman spectra on bulk samples were run on a Nicolet 910 FT Raman spectrometer equipped with a Nd:YAG laser (1064 nm). Typically, only 20 scans with a low laser power of around 20 mW were accumulated because longer exposure times or higher laser powers resulted in desorption of guest molecules and the deposition of bulk mercury halides on the glass capillary, giving rise to the observation of Raman spectra corresponding to those of the bulk halides. For microscopic Raman spectroscopy on individual crystallites, a Dilor spectrometer equipped with an attached microscope unit, a triple monochromator and a CCD recording unit were used. The applied laser wavelength was 632.4 nm.

Acknowledgements

This work has been supported by the Deutsche Forschungsgemeinschaft (Be 1664/1-1, 1-2 and 6-1) and the Fonds der Chemischen Industrie. B.P. gratefully acknowledges the Freistaat Bayern for a Ph.D. scholarship. Further we acknowledge the HASYLAB Hamburg for allocating measuring time and the kind assistance of HASYLAB staff, especially M. Tischer, L. Tröger and J. Feldhaus, during the measurements.

[1] "Solid-state Supramolecular Chemistry: Two- and Three-Dimensional Inorganic Networks", *Comprehensive Supramolecular Chemistry, Vol. 7* (Eds.: J. L. Atwood, D. D. MacNicol, J. E. D. Davies, F. Vögtle; G. Alberti, T. Bein), Pergamon, Oxford, **1996**.
[2] G. D. Stucky, J. E. Mac Dougall, *Science* **1990**, *247*, 669.
[3] P. Behrens, G. D. Stucky in *Comprehensive Supramolecular Chemistry*, *Vol. 7* (Eds. J. L. Atwood, D. D. MacNicol, J. E. D. Davies, F. Vögtle) Pergamon, Oxford, **1996**, pp. 721 – 772.
[4] G. A. Ozin, *Adv. Mater.* **1992**, *4*, 612.
[5] G. Schulz-Ekloff, D. Wöhrle, B. van Duffel, R. A. Schoonheydt, *Microporous Mesoporous Mater.* **2002**, *51*, 91.
[6] G. A. Ozin, C. Gil, *Chem. Rev.* **1989**, *89*, 1749 – 1764.
[7] P. Behrens, C. Panz, V. Hufnagel, B. Lindlar, C. C. Freyhardt, G. van de Goor, *Solid State Ionics* **1997**, *101 – 103*, 229.
[8] a) S. D. Cox, T. E. Gier, G. D. Stucky, J. Bierlein, *J. Am. Chem. Soc.* **1988**, *110*, 2986 – 2987; b) S. D. Cox, T. E. Gier, G. D. Stucky, *Chem. Mater.* **1990**, *2*, 609 – 619; c) L. Werner, J. Caro, G. Finger, J. Kornatowski, *Zeolites* **1992**, *12*, 658 – 663.
[9] M. E. Davis, R. F. Lobo, *Chem. Mater.* **1992**, *4*, 756; H. Kessler in *Comprehensive Supramolecular Chemistry, Vol. 7* (Eds. J. L. Atwood, D. D. MacNicol, J. E. D. Davies, F. Vögtle) Pergamon, Oxford, **1996**, pp. 425 – 464; S. L. Burkett, M. E. Davis, in *Comprehensive Supramolecular Chemistry*, *Vol. 7* (Eds. J. L. Atwood, D. D. MacNicol, J. E. D. Davies, F. Vögtle) Pergamon, Oxford **1996**, pp. 465 – 483.
[10] *Molecular Sieves: Science and Technology*, *Vol. 1*: *Synthesis* (Eds.: H. G. Karge, J. Weitkamp), Springer, Berlin, **1998**.
[11] a) G. A. Ozin, S. Özkar, *Adv. Mater.* **1992**, *4*, 11; b) G. A. Ozin, *Adv. Mater.* **1994**, *6*, 71; c) A. Corma, H. Garcia, *J. Chem. Soc. Dalton Trans.* **2000**, 1381 – 1394.

  0947-6539/02/0817-3936 $ 20.00+.50/0

[12] P. Behrens, G. van de Goor, M. Wark, A. Trnoska, A. Popitsch, *J. Mol. Struct.* **1995**, *348*, 85–90.
[13] G. Wirnsberger, H. P. Fritzer, A. Popitsch, G. van de Goor, P. Behrens, Angew. Chem. **1996**, *108*, 2951–2953; *Angew. Chem. Int. Ed. Engl.* **1996**, *35*, 2777–2779.
[14] G. Wirnsberger, H. P. Fritzer, G. van de Goor, B. Pillep, P. Behrens, A. Popitsch, *J. Mol. Struct.* **1997**, *410–411*, 123–127.
[15] G. Wirnsberger, H. P. Fritzer, H. Koller, P. Behrens, A. Popitsch, *J. Mol. Struct.* **1999**, *480–481*, 699–704.
[16] G. Wirnsberger, R. Zink, B. Pillep, H. P. Fritzer, A. Popitsch, P. Behrens, *J. Phys. Chem. B* **1999**, *103*, 5797–5801.
[17] P. Behrens, M. Hartl, G. Wirnsberger, A. Popitsch, B. Pillep, *Stud. Surf. Sci. Catal.* **2001**, *135*, 10-O-03.
[18] F. Liebau, H. Gies, R. P. Gunawardane, B. Marler, *Zeolites* **1986**, *6*, 373–377.
[19] Short terms for microporous tetrahedral frameworks are designated by the International Zeolite Association and can be found in: C. Baerlocher, W. M. Meier, D. H. Olson, *Atlas of Zeolite Structures Types*, 5th ed., Elsevier, Amsterdam, **2001**.
[20] The terms "channels" and "windows" are used synonymously for pore openings here. As is common in the structural description of zeotypes, only tetrahedral framework atoms are counted when the window aperture is given; oxygen bridges are omitted. Hence, "8-ring channel" classifies a pore-opening surrounded by eight tetrahedral units, that is eight Si and O atoms, each.
[21] a) P. Behrens, M. Alidoosti, F. Schulz, W. Metz, *Z. Naturforsch. B* **1989**, *44*, 721–728; b) P. Behrens, J. Ehrich, K. Lochte, W. Metz, W. Niemann, HASYLAB Annual Report 1989, HASYLAB/DESY, Hamburg **1990**, p. 241–242.
[22] a) J.-H. Choy, S.-J. Hwang, N. G. Park, *J. Am. Chem. Soc.* **1994**, *116*, 1624; b) J. H. Choy, N. G. Park, S. J. Hwang, D. H. Kim, N. H. Hur, *J. Am. Chem. Soc.* **1994**, *116*, 11564; c) J.-H. Choy, S.-J. Hwang, N. G. Park, *J. Am. Chem. Soc.* **1997**, *119*, 1624–1633; d) J.-H. Choy, W. Lee, S.-J. Hwang, *J. Mater. Chem.* **2000**, *10*, 1679–1684.
[23] The small channels can also be viewed as cages connecting the 10-rings, with their 8-ring windows perpendicular to the windows of the 10-ring channels.
[24] W. R. Wadt, *J. Chem. Phys.* **1980**, *72*, 2469–2478.
[25] P. Templet, J. R. McDonald, S. P. McGlynn, C. H. Kendrow, J. L. Roebber, K. Weiss, *J. Chem. Phys.* **1972**, *56*, 5746.
[26] T. R. Griffiths, R. A. Anderson, *J. Chem. Soc. Faraday Trans. II* **1979**, *75*, 957.
[27] Z. K. Tang, Y. Nozue, T. Goto, *J. Phys. Soc. Jpn.* **1992**, *61*, 2943–2950.
[28] R. Åkesson, I. Persson, M. Sandström, U. Wahlgren, *Inorg. Chem.* **1994**, *33*, 3715–3723.
[29] It may be considered, however, that in the case of oxidic compounds of Ag^{I} (as Hg^{II}, an oxidation state with a formally filled d^{10} sub-shell) similar pre-edge features in the AgL_3 XANES spectra were interpreted as arising from $2p_{3/2} \rightarrow 4d$ transitions (P. Behrens, *Solid State Commun.* **1992**, *81*, 235–239) and that theoretical investigations (M. Kaupp, H. G. von Schnering, *Inorg. Chem.* **1994**, *33*, 2555–2564) have shown that the $5d^{10}$ sub-shell of electrons is involved in chemical bonding in the HgX_2 compounds. An alternative assignment for the peaks under discussion here could thus be: *A*: $2p_{3/2} \rightarrow 5d$ and *B*: $2p_{3/2} \rightarrow 6s$ (P. Behrens, unpublished results). However, for the discussions presented here, the assignments are not important.
[30] D. E. Turner, B. N. Harmon, *Phys. Rev. B* **1989**, *40*, 10516–10522.
[31] T. Yamamura, T. Watanabe, A. Kikuchi, M. Ushiyama, T. Kobayashi, H. Hirota, *J. Phys. Chem.* **1995**, *99*, 5525–5531.
[32] In contrast, the UV/Vis spectra of iodine–DDR show a blue shift of the characteristic absorption upon lowering the temperature. This is readily explained in terms of electron donation from the framework oxygen atoms to the iodine guest molecules. G. Wirnsberger, A. Popitsch, P. Behrens, unpublished results.
[33] V. P. Spiridonov, A. G. Gershikov, B. S. Butayev, *J. Mol. Struct.* **1979**, *52*, 53; T. Yokoyama, K. Kobayashi, T. Ohta, A. Ugawa, *Phys. Rev. B* **1996**, *53*, 6111–6124.
[34] Y.-B. Dong, M. D. Smith, H.-C. zur Loye, *Angew. Chem.* **2000**, *112*, 4441–4443; *Angew. Chem. Int. Ed.* **2000**, *39*, 4271–4273.
[35] B. K. Teo, EXAFS: Basic Principles and Data Analysis, Springer, Berlin, **1988**.
[36] B. M. Pillep, Doctoral Thesis, Ludwig-Maximilians-Universität München (Germany), **1997**; B. M. Pillep, P. Behrens, unpublished results.
[37] I. Perrson, M. Sandström, P. L. Goggin, *Inorg. Chim. Acta*, **1987**, *129*, 183–197.
[38] G. Wirnsberger, P. Behrens, P. Knoll, unpublished results.
[39] R. D. Roders, A. H. Bond, J. L. Wolff, *J. Coord. Chem*. **1993**, *29*, 187–207 and references therein.
[40] G. Flachenecker, P. Behrens, G. Knopp, M. Schmitt, T. Siebert, A. Vierheilig, G. Wirnsberger, A. Materny, *J. Phys. Chem. A* **1999**, *103*, 3854–3863.
[41] M. Kaupp, H. G. von Schnering, *Inorg. Chem.* **1994**, *33*, 2555–2564.
[42] C. C. Freyhardt, M. Tsapatsis, R. F. Lobo, K. J. Balkus, M. E. Davis, *Nature* **1996**, *381*, 295–298.
[43] a) J. G. Eden, *Appl. Phys. Lett.* **1977**, *31*, 448–450; b) J. H. Parks, *Appl. Phys. Lett.* **1977**, *31*, 192–194; c) E. J. Schimitschek, J. E. Celto, J. A. Trias, *Appl. Phys. Lett.* **1977**, *31*, 608–610; d) R. Burnham, *Appl. Phys. Lett.* **1978**, *33*, 156–159.
[44] F. Laeri, private communication, **1999**.
[45] a) TON: J.-L. Guth, H. Kessler, J. M. Higel, J. M. Lamblin, J. Patarin, A. Sieve, J. M. Chezeau, R. Wey, *ACS Symp. Ser.* **1989**, *398*, 176; b) FER: A. Kuperman, S. Nadimi, S. Oliver, G. A. Ozin, *Nature* **1993**, *365*, 239–242; c) MFI: J. Patarin, M. Soulard, H. Kessler, J.-L. Guth, J. Baron, *Zeolites* **1989**, *9*, 397–404.
[46] T. Ressler, *J. Phys. IV France* **1997**, *7*, C2–269.; T. Ressler, *J. Synchrotron Rad.* **1998**, *5*, 118–122.
[47] W. H. McMaster, N. Kerr Del Grande, J. H. Mallet, J. H. Hubbel, Compilation of X-Ray Cross Sections, UCRL-50174 Sec. II Rev. 1, Lawrence Radiation Laboratory, University of California, Livermore, **1967**.
[48] S. I. Zabinsky, J. J. Rehr, A. Ankudinov, R. C. Albers, M. J. Eller, *Phys. Rev. B* **1995**, *52*, 2995–3009.
[49] H. Gies, *Z. Krist.* **1986**, *175*, 93.
[50] S. A. I. Barri, G. W. Smith, D. White, D. Young, *Nature* **1984**, *312*, 533; B. Marler, *Zeolites* **1987**, *7*, 393–397.
[51] R. E. Morris, S. J. Weigel, N. J. Henson, L. M. Bull, M. T. Janicke, B. F. Chmelka, A. K. Cheetham, *J. Am. Chem. Soc.* **1994**, *116*, 11849–11855; S. J. Weigel, J.-C. Gabriel, E. Guttierez Puebla, A. M. Bravo, N. J. Henson, L. M. Bull, A. K. Cheetham, *J. Am. Chem. Soc.* **1996**, *118*, 2427–2435; J. E. Lewis, C. C. Freyhardt, M. E. Davis, *J. Phys. Chem.* **1996**, *100*, 5039–5049.
[52] H. van Koningsveld, H. van Bekkum, J. C. Jansen, *Acta Crystallogr. B* **1987**, *43*, 127; H. van Koningsveld, *Acta Crystallogr. B* **1990**, *46*, 731; H. van Koningsveld, J. C. Jansen, H. van Bekkum, *Zeolites* **1990**, *10*, 235–242.
[53] G. A. Voyiatzis, G. N. Papatheodorou, *Ber. Bunsenges. Phys. Chem.* **1994**, *98*, 683–689.
[54] A. Chaves, R. S. Katiyar, S. P. S. Porto, *Phys. Rev. B* **1974**, 10, 3522–3533.

Received: September 5, 2001
Revised: May 16, 2002 [F3531]

  0947-6539/02/0817-3937 $ 20.00+.50/0